Electronic Relaxation Phenomena Following $^{57}Co(EC)^{57}Fe$ Nuclear Decay in $[Mn^{II}(terpy)_2](ClO_4)_2 \cdot {}^1/_2H_2O$ and in the Spin Crossover Complexes $[Co^{II}(terpy)_2]X_2 \cdot nH_2O$ (X = Cl and ClO_4): A Mössbauer Emission Spectroscopic Study‡

Hiroki Oshio,*,† Hartmut Spiering,§ Vadim Ksenofontov,§ Franz Renz,§ and Philipp Gütlich*,§

Department of Chemistry, Graduate School of Science, Tohoku University, Aoba-ku, Sendai 980-8578, Japan, and Institut für Anorganische Chemie und Analytische Chemie, Universität Mainz, Staudinger Weg 9, D-55099 Mainz, Germany

Received June 27, 2000

The valence states of the nucleogenic ^{57}Fe arising from the nuclear disintegration of radioactive ^{57}Co by electron capture decay, $^{57}Co(EC)^{57}Fe$, have been studied by Mössbauer emission spectroscopy (MES) in the ^{57}Co-labeled systems: $[^{57}Co/Co(terpy)_2]Cl_2 \cdot 5H_2O$ (**1**), $[^{57}Co/Co(terpy)_2](ClO_4)_2 \cdot {}^1/_2H_2O$ (**2**), and $[^{57}Co/Mn(terpy)_2](ClO_4)_2 \cdot {}^1/_2H_2O$ (**3**) (terpy = 2,2′:6′,2″-terpyridine). The compounds **1**, **2**, and **3** were labeled with ca. 1 mCi of ^{57}Co and were used as the Mössbauer sources at variable temperatures between 300 K and ca. 4 K. $[Fe(terpy)_2]X_2$ is a diamagnetic low-spin (LS) complex, independent of the nature of the anion X, while $[Co(terpy)_2]X_2$ complexes show gradual spin transition as the temperature is varied. The Co(II) ion in **1** "feels" a somewhat stronger ligand field than that in **2**; as a result, 83% of **1** stays in the LS state at 321 K, while in **2** the high-spin (HS) state dominates at 320 K and converts gradually to the LS state with a transition temperature of $T_{1/2} \approx 180$ K. Variable-temperature Mössbauer emission spectra for **1**, **2**, and **3** showed only LS-^{57}Fe(II) species at 295 K. On lowering the temperature, metastable HS Fe(II) species generated by the $^{57}Co(EC)^{57}Fe$ process start to grow at ca. 100 K in **1**, at ca. 200 K in **2**, and at ca. 250 K in **3**, reaching maximum values of 0.3 at 20 K in **1**, 0.8 at 50 K in **2**, and 0.86 at 100 K in **3**, respectively. The lifetime of the metastable HS states correlates with the local ligand field strength, and this is in line with the "inverse energy gap law" already successfully applied in LIESST relaxation studies.

Introduction

Electron capture (EC) decay of ^{57}Co in metal complexes gives rise to a variety of physical and chemical aftereffects, which can be most elegantly studied by Mössbauer emission spectroscopy.[1] Mössbauer emission spectra (MES) of ^{57}Co doped in Co(II) complexes with weak or intermediate ligand field strengths, for which the corresponding iron(II) compounds showed either HS behavior at all temperatures or temperature dependent spin crossover behavior, gave only HS-Fe(II) resonance lines over the entire temperature range.[2] On the other hand, MES of the ^{57}Co(II) complexes with relatively strong ligand fields, for which the corresponding iron(II) compounds showed LS behavior at all temperatures, revealed that metastable high-spin (HS) Fe(II) doublets were also observed in addition to a low-spin (LS) Fe(II) species. The intensity of the metastable HS-Fe(II) species was increasing on lowering the temperature. The time differential Mössbauer emission technique[3] has proven the HS-Fe(II) to be a metastable state after EC decay, which relaxes to the LS state. The metastable HS-Fe(II) state was for the first time observed in MES of $[^{57}Co/Co(phen)_3](ClO_4)_2$,[4] where the Fe(II) ion in the corresponding $[Fe(phen)_3](ClO_4)_2$ compound is in the $^1A_1$ ground state due to the fairly strong ligand field, but the Co(II) ion in $[Co(phen)_3](ClO_4)_2$ is in the HS $^4T_1$ ground state. At room temperature, the MES of $[^{57}Co/Co(phen)_3](ClO_4)_2$ shows only the poorly resolved doublet of the LS-Fe(II) state, while the additional doublet characteristic of HS-Fe(II) was observed at $\leq$200 K. The fraction of the HS-Fe(II) species increases as the temperature is lowered at the expense of the LS-Fe(II) fraction. This means, provided that the initial population does not depend on temperature, that the lifetime of the metastable HS-Fe(II) state is on the order of the Mössbauer time scale and becomes longer at cryogenic temperature. Approximately 10^{-9} s after the electron capture decay of $^{57}Co(EC)^{57}Fe$, the oxidation state of the nucleogenic ^{57}Fe is mainly 2+ and the electronic structure has decayed from highly excited electronic levels (Scheme 1) to the initial population of the $^1A_1$ ground state and the first $^5T_2$ excited state, the lifetime of which is on the order of the Mössbauer time scale and becomes longer at cryogenic temperature. A minor fraction of the nucleogenic $^{57}Fe^{3+}$ was also found in most of these MES

‡ Dedicated to Professor Dieter Sellmann on occasion of his 60th birthday.
† Tohoku University.
§ Universität Mainz.

(1) (a) Tuczek, F.; Spiering, H.; Gütlich, P. *Hyperfine Interact*. **1990**, *62*, 109. (b) Gütlich, P.; Ensling, J.; Tuczek, F. *Hyperfine Interact*. **1994**, *84*, 447. (c) Sato, T.; F. Ambe, T. Kitazawa, H. Sano, M. Takeda, *Chem. Lett*. **1997**, 1287. (d) Maeda, Y.; Oshio, H.; Takashima, Y. *Bull. Chem. Soc. Jpn*. **1982**, *55*, 3500. (e) Sano, H.; Gütlich P. In *Hot Atom Chemistry*; Matsuura, T., Ed.; Kodansha Ltd., Tokyo, 1984.

(2) (a) Ensling, J.; Gütlich, P.; Hasselbach, K. M.; Fitzsimmons, B. W. *Chem. Phys. Lett*. **1976**, *42*, 232. (b) Fleisch, J.; Gütlich, P. *Chem. Phys. Lett*. **1976**, *42*, 237. (c) Fleisch, J.; Gütlich, P. *Chem. Phys. Lett*. **1977**, *45*, 29.

(3) (a) Grimm, R.; Gütlich, P.; Kankeleit, E.; Link, R. *J. Chem. Phys.* **1977**, *67*, 5491. (b) Alflen, M.; Hennen, C.; Tuczek, F.; Spiering, H.; Gütlich, P.; Kajcsos, Z. *Hyperfine Interact.* **1989**, *47*, 115. (c) Hennen, C.; Alflen, M.; Spiering, H.; Gütlich, P. *Hyperfine Interact*. **1990**, *56*, 1527. (d) Deisenroth, S.; Hauser, A.; Spiering, H.; Gütlich, P. *Hyperfine Interact.* **1994**, *93*, 1573.

(4) Ensling, J.; Fitzsimmons, B. W.; Gütlich, P.; Hasselbach, K. M. *Angew. Chem*. **1970**, *82*, 638.

10.1021/ic000714a CCC: $20.00
Published on Web 02/13/2001

Scheme 1

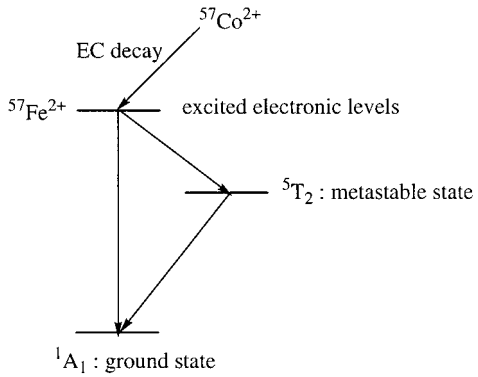

studies, which is believed to be due to incomplete electronic recombination and/or to redox processes following radiolysis in the ligand sphere.

The ^{57}Co(EC)^{57}Fe process may be regarded as an internal molecular excitation source, of which the energy release causes self-excitation leading to the population of excited electronic levels. This phenomenon has been termed NIESST (nuclear decay induced excited spin state trapping)[5] in analogy to the LIESST (light-induced excited spin state trapping)[6] phenomenon, the trapping of long-lived metastable states by external light irradiation. It has been well established that the thermally induced spin crossover behavior is very sensitive to chemical and physical effects like metal dilution,[7] counteranions,[8] solvent molecules,[9] external fields,[10] and applied pressure.[11] We have found that the lifetimes of the metastable HS states generated by ^{57}Co(EC)^{57}Fe are also affected by the ligand field strength and parent matrixes embedding the ^{57}Co atom. We report here the Mössbauer emission spectroscopic studies of [^{57}Co/Co(terpy)$_2$]Cl$_2$·5H$_2$O (**1**), [^{57}Co/Co(terpy)$_2$](ClO$_4$)$_2$·$^1/_2$H$_2$O (**2**), and [^{57}Co/Mn(terpy)$_2$](ClO$_4$)$_2$·$^1/_2$H$_2$O (**3**), where **1** and **2** are the first MES studies on cobalt(II) spin crossover complexes.

Experimental Section

Syntheses. Chemicals were purchased from Wakko Chemical Co. and were used without further purification. [Co(terpy)$_2$]Cl$_2$·5H$_2$O (**1m**), [Co(terpy)$_2$](ClO$_4$)$_2$·$^1/_2$H$_2$O (**2m**), [Mn(terpy)$_2$](ClO$_4$)$_2$·$^1/_2$H$_2$O (**3m**), and [Fe(terpy)$_2$](ClO$_4$)$_2$·$^1/_2$H$_2$O (**4m**) were prepared according to the reported methods.[12] Recrystallization of **2m**, **3m**, and **4m** from water gave dark red, pink, and dark red crystals, which were suitable for the X-ray structural analysis. ^{57}Co-labeled and ^{57}Fe-enriched complexes were prepared by using aqueous solutions of MCl$_2$·*n*H$_2$O (M = Co and Mn) doped with 1 mCi of ^{57}CoCl$_2$·6H$_2$O (Amersham Buchler) and enriched by 5 mol % of ^{57}FeCl$_2$·6H$_2$O, respectively.

Physical Measurements. Magnetic susceptibility data were collected in the temperature range 2.0−300 K and in an applied field of 10 kG of a Quantum Design model MPMS SQUID magnetometer. Pascal's constants were used to determine the diamagnetic corrections.[13] Mössbauer absorption spectra were obtained with a conventional spectrometer operated in constant acceleration mode. The principle of the resonance detector is based on the registration of electrons of internal conversion, appearing during the decay of excited resonance nuclear levels. Due to the great difference in efficiency of conversion electron registration on the one hand and γ- and X-rays on the other, the resonance detector counts practically only the conversion electrons, emitted after resonance absorption of recoilless γ-radiation. The resonance counter is very suitable for transitions with a high degree of conversion, which in the case of ^{57}Fe is 8.2. The generally high value of the signal/noise ratio is an important feature of the resonance detector. In our experiment the gas-filled counter with internal one-line-converter made of ^{57}Fe enriched stainless steel was used. This construction provides the signal/noise ratio of ca. 10:1. The absorber was encapsulated in a Plexiglas container and mounted in a cryostat for variable temperatures down to ca. 4 K. The ^{57}Co/Rh source (Wissel, Starnberg/Germany) was kept at room temperature. Mössbauer emission spectra were obtained by using the ^{57}Co-labeled complexes as a source at various temperatures. A homemade so-called resonance detector was employed, which operates as a conversion electron detector, whereby an unusually high counting efficiency is obtained by placing a ^{57}Fe-enriched stainless steel absorber inside the detector chamber. Counting efficiency is 10−20 times higher than with conventional detectors. Both the Mössbauer absorption and emission spectra were fitted. All the isomer-shift values in this report are given with respect to stainless steel at room temperature.

X-ray Structure Analyses. Each single crystal of **2m** (0.2 × 0.2 × 0.3 mm^3), **3m** (0.1 × 0.2 × 0.3 mm^3), and **4m** (0.25 × 0.3 × 0.3 mm^3) was mounted with epoxy resin on the tip of a glass fiber. Diffraction data were collected at −30 °C on a Bruker SMART 1000 diffractometer fitted with a CCD-type area detector, and a full sphere of data was collected by using graphite-monochromated Mo Kα radiation (λ = 0.71073 Å). At the end of data collection, the first 50 frames of data were re-collected to establish that the crystal had not deteriorated during the data collection. The data frames were integrated using SAINT and were merged to give a unique data set for the structure determination. Empirical absorption corrections by SADABS (G. M. Sheldrick, 1994) were carried out, and relative transmissions are 1.000−0.958, 1.000−0.997, and 1.000−0.966 for **2m**, **3m**, and **4m**, respectively. Totals of 7345 ($2° < \theta < 26°$), 14511 ($1° < \theta < 26°$), and 7345 ($2° < \theta < 26°$) reflections were respectively collected for **2m**, **3m**, and **4m**, which yield 1552 (R_{int} = 0.0433), 6075 (R_{int} = 0.0277), and 5600 (R_{int} = 0.0226) independent reflections, respectively. Crystallographic data are listed in Table 1. The structures were solved by direct methods and refined by the full-matrix least-squares method on all F^2 data using the SHELXTL 5.1 package (Bruker Analytical X-ray Systems). Non-hydrogen atoms were refined with anisotropic thermal parameters. Hydrogen atoms were included in calculated positions and refined with isotropic thermal parameters riding on those of the parent atoms.

Results

In the following sections, the ^{57}Co-labeled and the unlabeled complexes are numbered without and with a character **m**, respectively.

(5) (a) Gütlich, P.; Hauser, A.; Spiering, H. *Angew. Chem., Int. Ed. Engl.* **1994**, *33*, 2024. (b) Gütlich, P.; Hauser, A.; Spiering, H. *Angew. Chem.* **1994**, *106*, 2109. (c) Gütlich, P. *Mol. Cryst. Liq. Cryst.* **1997**, *305*, 17.

(6) (a) Decurtins, S.; Gütlich, P.; Köhler, C. P.; Spiering, H.; Hauser, A. *Chem. Phys. Lett.* **1984**, *105*, 1. (b) Decurtins, S.; Gütlich, P.; Köhler, C. P.; Spiering, H.; Hauser, A. *Inorg. Chem.* **1985**, *24*, 2174. (c) Hauser, A. *J. Chem. Phys.* **1991**, *94*, 2741. (d) Hauser, A. *Comments Inorg. Chem.* **1995**, *17*, 17.

(7) (a) Sorai, M.; Ensling, J.; Gütlich, P. *Chem. Phys.* **1976**, *18*, 199. (b) Spiering, H.; Meissner, E.; Köppem, H.; Müller, E. W.; Gütlich, P. *Chem. Phys.* **1982**, *68*, 65.

(8) (a) Renovitch, G. A.; Baker, W. A., Jr. *J. Am. Chem. Soc.* **1967**, *89*, 6377. (b) Wiehl, L.; Kiel, G.; Köhler, C. P.; Spiering, H.; Gütlich, P. *Inorg. Chem.* **1986**, *5*, 1565.

(9) (a) Sorai, M.; Ensling, J.; Hasselbach, K. M.; Gütlich, P. *Chem. Phys.* **1977**, *20*, 197. (b) Gütlich, P.; Köppen, H.; Steinhäuser, H. G. *Chem. Phys. Lett.* **1980**, *74*, 3.

(10) Qi, Y.; Müller, E. W.; Spiering, H.; Gütlich, P. *Chem. Phys. Lett.* **1983**, *101*, 503.

(11) (a) Meissner, E.; Köppen, H.; Spiering, H.; Gütlich, P. *Chem. Phys. Lett.* **1983**, *95*, 163. (b) Köhler, C. P.; Jakobi, R.; Meissner, E.; Wiehl, L.; Spiering, H.; Gütlich, P. *J. Phys. Chem. Solids* **1990**, *51*, 239.

(12) (a) Baker, A. T.; Goodwin, H. A. *Aust. J. Chem.* **1985**, *38*, 207. (b) Figgis, B. N.; Kucharski, E. S.; White, A. H. *Aust. J. Chem.* **1983**, *36*, 1527. (c) Figgis, B. N.; Kucharski, E. S.; White, A. H. *Aust. J. Chem.* **1983**, *36*, 1537. (d) Figgis, B. N.; Kucharski, E. S.; White, A. H. *Aust. J. Chem.* **1983**, *36*, 1563.

(13) Hatfield, W. E. In *Theory and Application of Molecular Paramagnetism*; Boudreaux E. A., Mulay, L. N., Eds.; Wiley and Sons: New York, 1976; 491−495.

Table 1. Crystallographic Data for $[M(terpy)_2](ClO_4)_2 \cdot {}^1/_2H_2O$

	$[Co(terpy)_2](ClO_4)_2 \cdot {}^1/_2H_2O$ (**2m**)	$[Mn(terpy)_2](ClO_4)_2 \cdot {}^1/_2H_2O$ (**3m**)	$[Fe(terpy)_2](ClO_4)_2 \cdot {}^1/_2H_2O$ (**4m**)
chem formula	$C_{30}H_{23}Cl_2CoN_6O_8$	$C_{30}H_{23}Cl_2MnN_6O_9$	$C_{30}H_{23}Cl_2FeN_6O_8$
fw	724.37	736.38	722.29
temp (°C)	−30	−30	−30
cryst syst	tetragonal	tetragonal	monoclinic
space group	*P*4(2)/*n*	*P*4(3)	*P*2(1)
a (Å)	8.849(2)	8.8079(3)	8.8102(6)
b (Å)			8.8967(6)
c (Å)	20.076(5)	40.035(2)	19.923(1)
β (deg)			100.712(1)
vol (Å^3)	1571.9(6)	3105.8(2)	1534.4(2)
Z	2	4	2
ρ_{calcd} (Mg/m^3)	1.530	1.575	1.563
μ (mm^{-1})	0.776	0.663	0.728
λ, (Å)	0.71073	0.71073	0.71073
final *R* indices[a]	R1 0.0349	R1 0.0507	R1 0.0435
[$I > 2\sigma(I)$]	wR2 0.0774	wR2 0.1235	wR2 0.1115

[a] $R1 = \sum||F_o| - |F_c||/\sum|F_o|$. $wR2 = [\sum[w(F_o^2 - F_c^2)^2]/\sum[w(F_o^2)^2]]^{0.5}$. Calcd $w = 1/[\sigma^2(F_o^2) + (0.0520P)^2 + 0.000P]$ for **2m**, $w = 1/[\sigma^2(F_o^2) + (0.0639P)^2 + 3.0103P]$ for **3m**, and $w = 1/[\sigma^2(F_o^2) + (0.0847P)^2 + 0.726P]$ for **4m**, where $P = (F_o^2 + 2F_c^2)/3$.

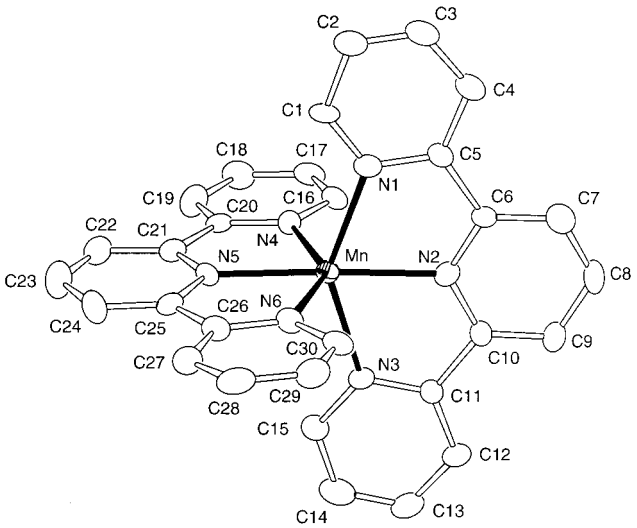

Figure 1. ORTEP diagram of $[Mn(terpy)_2]^{2+}$ with 30% of thermal ellipsoids.

Structures of $[Co(terpy)_2](ClO_4)_2 \cdot {}^1/_2H_2O$ (2m), $[Mn(terpy)_2](ClO_4)_2 \cdot {}^1/_2H_2O$ (3m), and $[Fe(terpy)_2](ClO_4)_2 \cdot {}^1/_2H_2O$ (4m). The X-ray structure analyses for **2m**[14] and **4m**[15] have already been reported. In this study, we found that the Mössbauer emission spectra for ^{57}Co in **2m** and **3m** shows quite a different temperature dependence. Therefore, we decided to reinvestigate the structure analyses of our samples, and the crystals of **2m** and **4m** prepared in this study were confirmed to be isomorphous with the reported complexes. The structure of the cation **3m** is depicted in Figure 1.

The metal ions in **2m**, **3m**, and **4m** have pseudo-octahedral coordination geometry, and six coordination sites are occupied by nitrogen atoms from the terpy ligand. The coordination bond lengths between Co^{2+}, Mn^{2+}, and Fe^{2+} ions and the coordinated nitrogen atoms are in the ranges 2.022(3)−2.141(2) Å, 2.213(6)−2.263(5) Å, and 1.888(3)−1.990(3) Å, serially.

Magnetic Properties. A series of $[Co(terpy)_2]X_2$ has been reported to show the thermally induced spin transition between ^{2}E (LS) and $^4T_1$ (HS) states. The temperature dependence of the magnetic behavior, which has been reported down to liquid nitrogen temperature, depends on the counteranions and solvent molecules.[16] Temperature dependent magnetic susceptibilities for $[Co(terpy)_2]Cl_2 \cdot 5H_2O$ (**1m**) and $[Co(terpy)_2](ClO_4)_2 \cdot {}^1/_2H_2O$ (**2m**) have been reinvestigated by us down to 2.0 K, and the temperature dependences of the HS fractions calculated by the simple additive property of the susceptibilities are depicted in Figure 2.

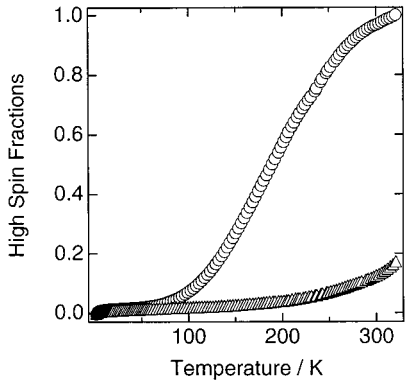

Figure 2. Temperature dependence of the HS fraction in (△) $[Co(terpy)_2]Cl_2 \cdot 5H_2O$ and (○) $[Co(terpy)_2](ClO_4)_2 \cdot {}^1/_2H_2O$.

The $\chi_m T$ value at 322 K for **2m** is 2.30 emu mol^{-1} K, which would be an expected value for the isolated HS Co(II) ($S = {}^3/_2$) ion with $g = 2.022$. The $\chi_m T$ values for **2m** gradually decrease as the temperature is lowered, and more than 96% goes to the LS states below ca. 80 K. On the other hand, the $\chi_m T$ value at 321 K for **1m** is 0.68 emu mol^{-1} K, which corresponds to 83% of **1m** being in the LS state. As the temperature is lowered, 96% of **1m** is in the LS state at 200 K and the $\chi_m T$ reaches the minimum value of 0.42 emu mol^{-1} K at 2.0 K. In accord with the lower spin-pairing energy for the Fe(II) ion compared with that for the Co(II) ion, $[Fe(terpy)_2](ClO_4)_2 \cdot {}^1/_2H_2O$ (**4m**) is diamagnetic (LS), while $[Mn(terpy)_2](ClO_4)_2 \cdot {}^1/_2H_2O$ (**3m**) is in the HS state with $S = {}^5/_2$.

Mössbauer Spectroscopic Studies. Mössbauer absorption spectra (MAS) for $[^{57}Fe_{0.05}Co_{0.95}(terpy)_2]Cl_2 \cdot 5H_2O$, $[^{57}Fe_{0.05}Co_{0.95}(terpy)_2](ClO_4)_2 \cdot {}^1/_2H_2O$, and $[^{57}Fe_{0.05}Mn_{0.95}(terpy)_2](ClO_4)_2 \cdot {}^1/_2H_2O$ at variable temperatures were measured, and Mössbauer

(14) Figgis, B. N.; Kucharski, E. S.; White, A. H. *Aust. J. Chem*. **1983**, *36*, 1537.
(15) Baker, A. T.; Goodwin, H. A. *Aust. J. Chem*. **1985**, *38*, 207.
(16) (a) Hogg, R.; Wilkins, R. G. *J. Chem. Soc*. **1962**, 341. (b) Schmidt, J. G.; Brey, W. S., Jr.; Stoufer, R. C. *Inorg. Chem*. **1967**, *6*, 268. (c) Figgis, B. N.; Kucharski, E. S.; White, A. H. *Aust. J. Chem*. **1983**, *36*, 1537. (d) Figgis, B. N.; Kucharski, E. S.; White, A. H. *Aust. J. Chem*. **1983**, *36*, 1527.

Table 2. Selected Parameters of Mössbauer Absorption and Emission Spectra

		low-spin Fe(II)			high-spin Fe(II)					
					HS1[a]			HS2[a]		
compound	temp (K)	IS (mm s^{-1})	QS (mm s^{-1})	S[b] (%)	IS (mm s^{-1})	QS (mm s^{-1})	S[b] (%)	IS (mm s^{-1})	QS (mm s^{-1})	S[b] (%)
[^{57}Fe/Co(terpy)$_2$]Cl$_2$	300	0.19	1.01							
	80	0.27	1.00							
[^{57}Fe/Co(terpy)$_2$](ClO$_4$)$_2$	300	0.21	1.00							
	80	0.28	1.00							
[^{57}Fe/Mn(terpy)$_2$](ClO$_4$)$_2$	300	0.23	0.98							
	80	0.31	0.95							
[^{57}Co/Co(terpy)$_2$]Cl$_2$ (**1**)	295	0.22	1.08							
	150	0.28	1.07							
	100	0.29	1.07	96	1.12	1.30	1	0.70	3.00	3
	70	0.30	1.07	89	1.09	1.30	8	0.76	3.21	3
	4.5	0.30	1.05	68	1.02	1.28	30	0.58	2.89	2
[^{57}Co/Co(terpy)$_2$](ClO$_4$)$_2$ (**2**)	295	0.24	1.06							
	250	0.26	1.06	98				0.90	2.52	2
	200	0.28	1.05	93	1.02	1.45	2	0.90	2.48	5
	150	0.30	1.04	76	1.03	1.59	15	0.91	2.64	9
	100	0.30	1.05	33	1.02	1.85	59	0.94	2.77	8
	4.5	0.30	1.09	13	1.02	1.95	79	0.93	2.82	8
[^{57}Co/Mn(terpy)$_2$](ClO$_4$)$_2$ (**3**)	295	0.26	1.03							
	250	0.28	1.02	78	1.06	1.21	17	1.04	1.91	4
	200	0.29	1.02	50	1.00	1.62	48	1.05	2.35	2
	150	0.29	1.15	19	1.03	1.93	78	1.08	2.55	3
	100	0.27	1.32	13	1.06	2.08	84	1.08	2.65	3
	4.5	0.25	1.39	11	1.07	2.13	86	1.09	2.72	4

[a] HS1 and HS2 are long- and short-lived species generated by EC-decay, respectively. [b] High-spin or low-spin fractions estimated from Mössbauer peak area.

emission spectra (MES) for [^{57}Co/Co(terpy)$_2$]Cl$_2$·5H$_2$O (**1**), [^{57}Co/Co(terpy)$_2$](ClO$_4$)$_2$·$^1/_2$H$_2$O (**2**), and [^{57}Co/Mn(terpy)$_2$](ClO$_4$)$_2$·$^1/_2$H$_2$O (**3**) were measured as Mössbauer sources at different temperatures using a so-called conversion electron resonance detector with a built-in ^{57}Fe-enriched stainless steel foil as Mössbauer scatterer at room temperature. Detailed values of the Mössbauer parameters resulting from the least-squares fitting procedures are listed in Table 2 for a representative set of temperatures. The MAS of ^{57}Fe embedded in the different matrixes under study revealed that the Fe^{2+} ions are LS over the whole temperature range in all cases; the isomer shifts (IS: 0.19−0.31 mm s^{-1}) are characteristic of LS-Fe(II) with quadrupole splittings of QS ≈ 0.95−1.01 mm s^{-1}.[17]

MES for **1**, **2**, and **3** are depicted in Figures 3 and 4, and temperature variations of the HS and LS fractions are shown in Figure 5. MES of **1**−**3** at 295 K consist of a single quadrupole doublet (LS) assigned to the LS-Fe(II), which was identified as the ground state by comparison with the very same parameters derived from the MAS of [^{57}Fe$_{0.05}$Co$_{0.95}$(terpy)$_2$]Cl$_2$·5H$_2$O. On lowering of the temperature, **1**−**3** show two additional doublets denoted as HS1 and HS2. The values of the isomer shift IS and the quadrupole splitting QS for HS1 and HS2 are characteristic of HS-Fe(II) ions (Table 2).[15] HS1 in **1**−**3** shows variable fractions with temperature, and the temperature behavior depends on the parent matrixes. The HS2 fractions in **1**−**3** are relatively small and do not change so much within the experimental error. HS1 peaks in MES for **1**, **2**, and **3** start to grow at 100, 200, and 250 K in the direction of the decreasing temperature, and the fractions reach their plateau values of 0.3, 0.79, and 0.86 at 20, 50, and 100 K, serially, whereas the LS fractions for **1**−**3** at 4.2 K are 0.68, 0.13, and 0.11, respectively. The data are plotted in Figures 3, 4, and 5.

(17) (a) Greenwood, N. N.; Gibb, T. C. *Mössbauer Spectroscopy*; Chapman and Hall Ltd., London, 1971. (b) Gütlich, P.; Link, R.; Trautwein, A. X. *Mössbauer Spectroscopy and Transition Metal Chemistry*; Springer: Berlin, Heidelberg, New York, 1978.

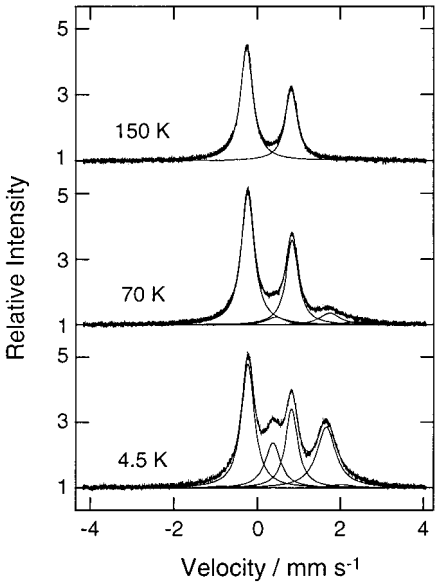

Figure 3. Selected Mössbauer emission spectra of [^{57}Co/Co(terpy)$_2$]Cl$_2$·5H$_2$O.

Discussion

Earlier MES studies of the valence states of nucleogenic ^{57}Fe generated by the electronic capture decay of ^{57}Co, ^{57}Co(EC)^{57}Fe, embedded in MN$_6$ core complexes with Schiff base ligands of different field strengths yielded, with the exception of a small and temperature independent fraction of $^{57}Fe^{3+}$ signals, mainly resonances characteristic of iron(II) LS and HS states. At a very early stage of such MES studies one has already found that the resonance intensities of these states and their temperature dependences could be correlated with the ligand field strength: ^{57}Co-labeled weak and intermediate field strength complexes, whose iron(II) analogues show HS behavior at all temperatures or undergo temperature dependent spin transition as confirmed

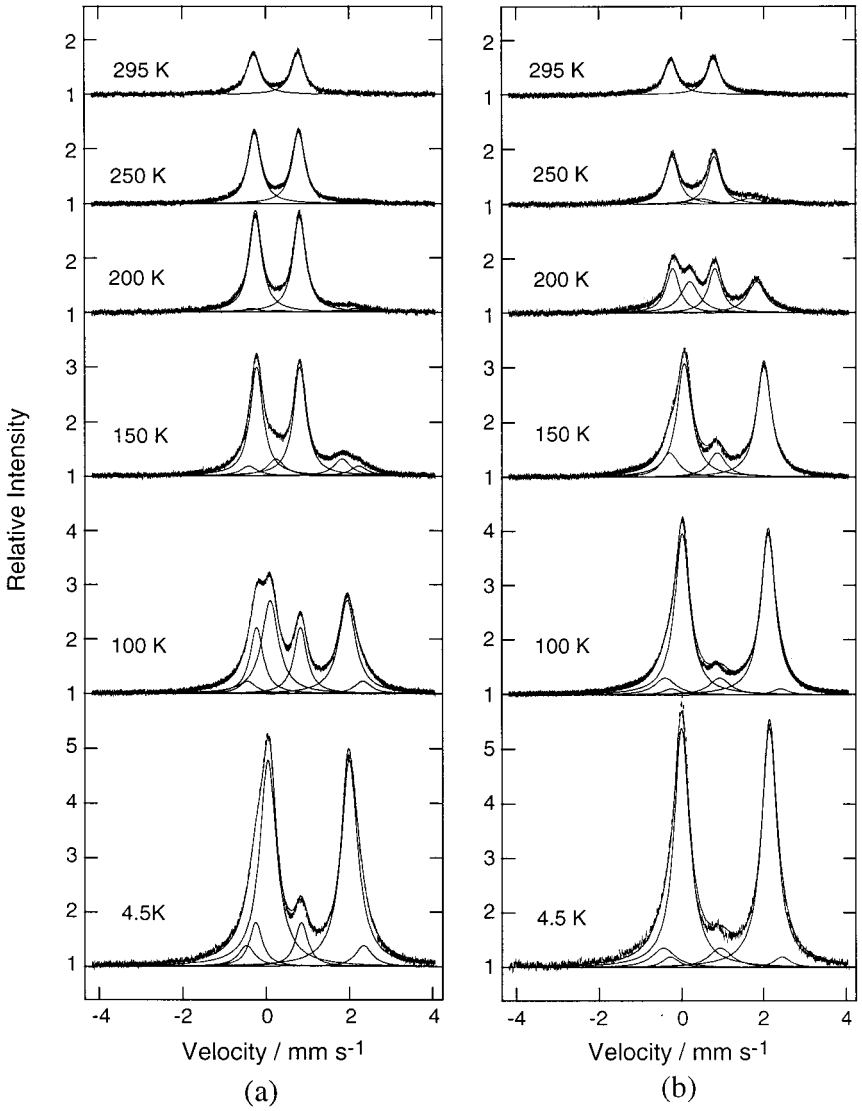

Figure 4. Selected Mössbauer emission spectra of (a) $[^{57}Co/Co(terpy)_2](ClO_4)_2 \cdot {}^1/_2H_2O$ and (b) $[^{57}Co/Mn(terpy)_2](ClO_4)_2 \cdot {}^1/_2H_2O$.

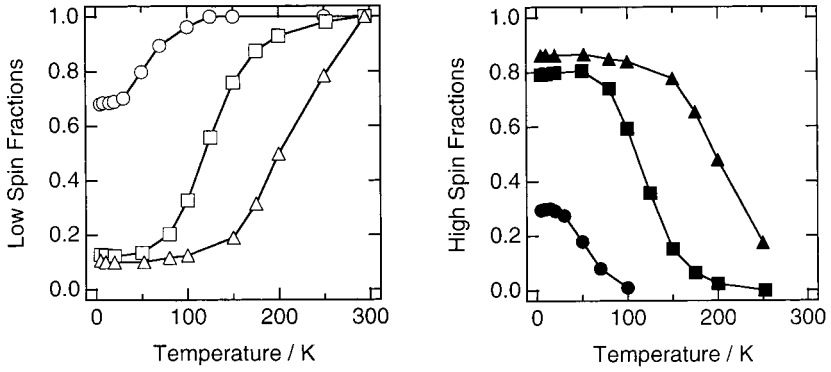

Figure 5. Temperature dependence of the low-spin (open mark) and high-spin (HS1) (filled mark) fractions observed in of (○) $[^{57}Co/Co(terpy)_2]Cl_2 \cdot 5H_2O$, (□) $[^{57}Co/Co(terpy)_2](ClO_4)_2 \cdot {}^1/_2H_2O$, and (△) $[^{57}Co/Mn(terpy)_2](ClO_4)_2 \cdot {}^1/_2H_2O$.

by, e.g., Mössbauer absorption spectroscopy, yield only ^{57}Fe(II)-HS doublets over the whole temperature under study.[2] ^{57}Co-labeled strong-field complexes such as $[^{57}Co/Co(phen)_3](ClO_4)_2$ or $[^{57}Co/Co(bipy)_3](ClO_4)_2$,[3,4] (phen = 1,10-phenanthroline; bipy= 2,2′-dipyridyl), whose analogous iron(II) compounds are typical examples for temperature independent LS behavior, yield MES spectra consisting of only LS-Fe(II) resonance signals at room temperature. HS-Fe(II) doublets appear with increasing intensity on lowering of the temperature, e.g., below 220 K in the case of $[^{57}Co/Co(phen)_3](ClO_4)_2$. These two additional HS-Fe(II) doublets besides the stable LS-Fe(II) state were proposed to be metastable states generated by the EC decay. Further Mössbauer emission experiments by means of the time-differential technique (TDMES)[3] revealed that the

metastable HS-Fe(II) states observed in $[^{57}Co/Co(phen)_3](ClO_4)_2$ relax to the LS-Fe(II) state. The lifetimes of the HS states increased as the temperature was lowered, and one of the HS-Fe(II) states relaxed much faster (lifetime of 645 ns at 10 K) than the other ($>10^4$ ns). On the other hand, the light irradiation of the LS-Fe(II) complex of $[Fe(phen)_3]^{2+}$ can convert the spin state of the Fe(II) ion from the LS to the HS state, which is termed LIESST, and the light-induced excited HS state relaxes back to the LS state. The application of the pulsed-laser technique on $[Fe(phen)_3]^{2+}$ embedded in a Nafion matrix enabled one to estimate the lifetime of the light-induced excited HS states, and the rate constant $k_{HL}(T\rightarrow 0)$ of ca. 5×10^6 s^{-1}[18] is comparable to the reciprocal value of the lifetime for the short-lived HS state in $[^{57}Co/Co(phen)_3](ClO_4)_2$ as determined by TDMS. Similar MES studies, both time-integral and time-differential, were performed later by Deisenroth et al.[3] on a single crystal of $[^{57}Co/Mn(bipy)_3](PF_6)_2$. The measured lifetimes of the metastable HS states of $^{57}Fe(II)$ were again, within experimental error limits, the same as those determined of the short-lived LIESST states after irradiation with an external light source. We have therefore concluded that the metastable HS-Fe(II) states generated by nuclear decay of $^{57}Co(II)$—now termed nuclear decay induced excited spin state trapping (NIESST)—are the same as those generated in a LIESST experiment. It is noted that in $[^{57}Co/Co(phen)_3](ClO_4)_2$ the fraction of the short-lived HS fraction increased as the temperature was lowered at the expense of the LS-Fe(II) species, while the long-lived HS fraction was temperature independent. The origin of the long-lived HS-Fe(II) state in MES, which might result from a defect caused by radiolysis, is unclear. The temperature dependence of the HS-Fe(II) fractions and the Mössbauer parameters derived from the emission spectra of $[^{57}Co/Co(terpy)_2]Cl_2 \cdot 5H_2O$ (**1**), $[^{57}Co/Co(terpy)_2](ClO_4)_2 \cdot {}^1/_2H_2O$ (**2**), and $[^{57}Co/Mn(terpy)_2](ClO_4)_2 \cdot {}^1/_2H_2O$ (**3**) must be viewed on the same grounds as the earlier studies on the ^{57}Co-labeled phen and bipy complexes; the HS1 and HS2 can be assigned to the short- and long-lived metastable HS-Fe(II) species, respectively.

The temperature dependencies of the HS1 factions in **1**−**3** are dependent on the parent matrixes. The HS1 in **1** starts to grow at 100 K and reaches a maximum value of 0.3 at 20 K, while in **2** it appears at 200 K and increases its fraction to the plateau (0.79) at 50 K. This temperature behavior of HS1 means that the lifetime in **1** is shorter than in **2**. The reason is that the ligand field strength in **1** is stronger than in **2** as can be seen from the magnetic susceptibility data for $[Co(terpy)_2]Cl_2 \cdot 5H_2O$ (**1m**) and $[^{57}Co/Co(terpy)_2](ClO_4)_2 \cdot {}^1/_2H_2O$ (**2m**) which show a higher HS fraction for **2** at all temperatures than for **1.** The two-potential-well Scheme 2 for an iron(II) spin crossover system[5] visualizes the correlation between the relaxation rate of the HS1 state and the ligand field strength: the stronger the ligand field, the larger the energy difference $\Delta E_{HL}{}^o$ between the lowest vibronic levels of the HS and LS states and the faster the relaxation of the metastable HS1 state (or equivalently the shorter its lifetime). This is known as "inverse energy gap law". This explains the faster relaxation of the metastable HS1 state in **1** as compared to **2**.

Scheme 2

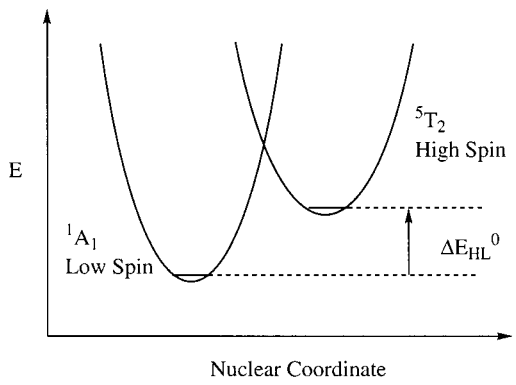

The MES of **3** showed the longest lifetimes of the HS1 species among the compounds studied. The HS1 state in **3** has already appeared at 250 K, and its fraction reached the plateau value of 0.86 at 100 K. It should be noted that the $^{57}Co(II)$ ions in **1m** and **2m** were imbedded in the cobalt complexes, while the $^{57}Co(II)$ ion was doped into the $[Mn(terpy)_2](ClO_4)_2 \cdot {}^1/_2H_2O$ (**3m**). Whereas the ligand field strengths at the ^{57}Co ions in **1m** and **2m** are exactly the same as at the nonradioactive Co(II) ions, a relative ligand field strength of the $^{57}Co(II)$ ion in **3m** cannot be estimated. It can only be concluded from the MES that it must be somewhat weaker than in **1** and **2**.

Spin crossover behavior, in which cooperative interactions must be involved, is influenced by many factors. Internal and external pressure effects are one of the major effects and have been extensively studied in several ferrous spin crossover systems, e.g., $[Fe(2\text{-pic})_3]Cl_2$ (2-pic = 2-picolylamine).[11] The size of the molecule in the LS state is smaller than that in the HS state, which has been proved by X-ray structural analyses;[19] hence, the increase in pressure will favor the LS state and the spin transition occurs at the higher temperature under the elevated pressure. Variable-pressure and -temperature Mössbauer experiments for $[Fe(2\text{-pic})_3]Cl_2 \cdot EtOH$ revealed that the spin transition temperature was shifted toward higher temperature with increasing pressure.[11] Incorporation of the spin crossover complex into a similar host lattice results in a similar pressure effect. Metal dilution experiments on $[Fe(2\text{-pic})_3]Cl_2 \cdot EtOH$ and $[Fe(phen)_2(NCS)_2]$ to host lattices of $[Zn(2\text{-pic})_3]Cl_2 \cdot EtOH$ and $[Mn(phen)_2(NCS)_2]$, respectively, with larger spacings (lattice parameters) as compared to the corresponding iron compounds revealed that such dilution leads to the stabilization of the HS states and lowered the spin transition temperature. This phenomenon has been described as a negative image pressure effect.[7] The metastable species of $[^{57m}Fe(terpy)_2]^{2+}$ generated after EC-decay are supposed to experience similar pressure effects. It is difficult to predict the magnitude of the image pressure on $[^{57m}Fe(terpy)_2]^{2+}$ in the different matrixes of **2m** and **3m** because **2m**, **3m**, and $[Fe(terpy)_2](ClO_4)_2 \cdot {}^1/_2H_2O$ (**4m**) crystallize in the different space groups of $P4_2/n$, $P4_3$, and $P2_1$, respectively. It should be noted, however, that the crystal systems of **2m** and **3m** are tetragonal and the unit cell volume of **3m** is twice that of **2m**. Despite the near-doubling of the lattice constant *c*, the packings of **2m** and **3m** are similar (Figure 6).

The cell volume of **2m** is 1571.9 Å^3 ($Z = 2$), while that of **3m** is 3105.8(2) Å for $Z = 4$ (or 1559.2 Å^3 converted for $Z = 2$). The molar volumes for **2m**, **3m**, and **4m** are estimated to be 786.0, 776.5, and 762.2 Å^3/mol, respectively, from the X-ray data. The metastable $[^{57m}Fe(terpy)_2]^{2+}$ species is considered to experience the negative pressure in **2** and **3**, the former giving the more negative pressure. EMS of **3** is, therefore, expected to give the shorter-lived HS1 species; however, the longer-lived HS1 in **3** was observed. It seems that the image pressure effect is not the only important factor. Recently, J. Kusz et al.

(18) (a) Vef, A. Dissertation, Universität Mainz, 1993. (b) Hauser, A. *Chem. Phys. Lett.* **1990**, *173*, 507.
(19) (a) Mikami, M.; Konno, M.; Saito, Y. *Acta Crystallogr.* **1980**, *B36*, 275. (b) Wiehl, L.; Kiel, G.; Köhler, C. P.; Spiering, H.; Gütlich, P. *Inorg. Chem.* **1986**, *25*, 1565.

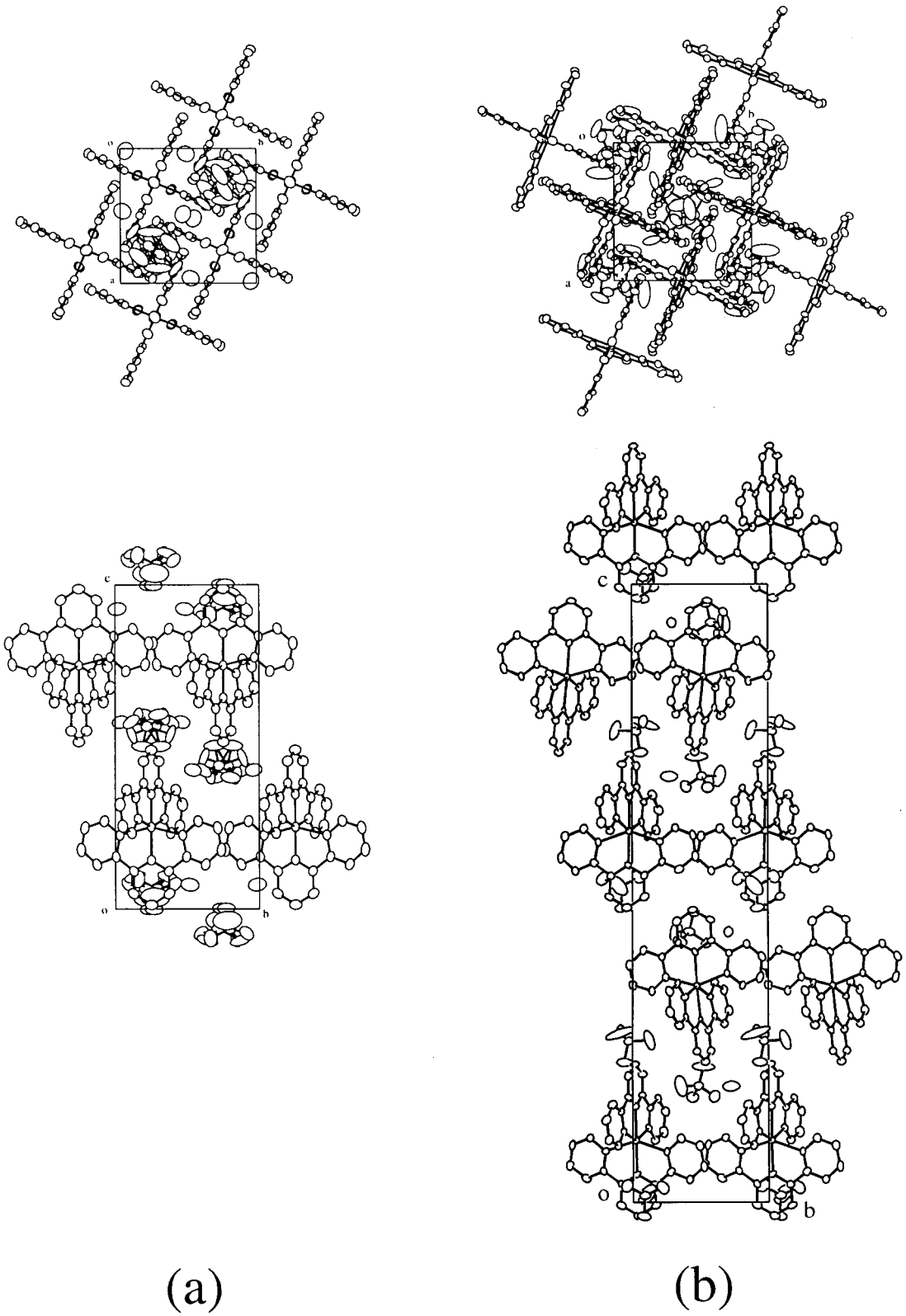

Figure 6. Perspective views on *bc*- and *ac*-planes for (a) $[Co(terpy)_2](ClO_4)_2 \cdot {}^1/_2H_2O$ and (b) $[Mn(terpy)_2](ClO_4)_2 \cdot {}^1/_2H_2O$.

performed structural studies after and before LIESST on the spin crossover system $[Fe(mtz)_6](BF_4)_2$ (mtz = 1-methyltetrazole).[20] They observed a drastic deformation of the unit cell after the light conversion from the HS to LS states, but there is not a measurable volume change after LIESST. From the elasticity theory, the volume change contributes the elastic energy, but the deformation is much more effective. In our EMS system, such deformation effects might be more effective than the image pressure effect.

Conclusion

In Fe(II) spin crossover systems, chemical modification and physical treatments of the complexes result in different spin crossover behaviors. Mössbauer emission spectroscopic studies

(20) Kusz, J.; Spiering, H.; Renz, F.; Gütlich, P. To be published.

on ^{57}Co doped in manganese and spin crossover cobalt complexes with terpy ligands revealed that the lifetimes of metastable iron(II) HS states generated by EC-decay are sensitive to the parent matrixes and the ligand field strength, where the stronger ligand field strength leads to the shorter lifetime of the metastable states in full agreement with the "inverse energy gap law" in the frame of nonadiabatic electronic relaxation.

Acknowledgment. This work was in part supported by Izumi Science and Technology Foundation and a Grant in aid for Scientific Research from the Ministry of Education, Science, and Culture, Japan. We also thank the Fonds der chemischen Industrie and the University of Mainz (MWFZ) for financial support.

Supporting Information Available: X-ray crystallographic files in CIF format for **2m**, **3m**, and **4m**. This material is available free of charge via the Internet at http://pubs.acs.org.

IC000714A